We are IntechOpen, the world's leading publisher of Open Access books Built by scientists, for scientists

4,800
Open access books available

122,000
International authors and editors

135M
Downloads

Our authors are among the

154
Countries delivered to

TOP 1%
most cited scientists

12.2%
Contributors from top 500 universities

CLARIVATE ANALYTICS BOOK CITATION INDEX INDEXED

WEB OF SCIENCE™

Selection of our books indexed in the Book Citation Index in Web of Science™ Core Collection (BKCI)

Interested in publishing with us?
Contact book.department@intechopen.com

Numbers displayed above are based on latest data collected.
For more information visit www.intechopen.com

5

Finite Volume Method Analysis of Heat Transfer in Multi-Block Grid During Solidification

Eliseu Monteiro[1], Regina Almeida[2] and Abel Rouboa[3]
[1]*CITAB/UTAD - Engineering Department of University of Trás-os-Montes e Alto Douro, Vila Real*
[2]*CIDMA/UA - Mathematical Department of University of Trás-os-Montes e Alto Douro, Vila Real*
[3]*CITAB/UTAD - Department of Mechanical Engineering and Applied Mechanics of University of Pennsylvania, Philadelphia, PA*
[1,2]*Portugal*
[3]*USA*

1. Introduction

Solidification of an alloy has many industrial applications, such as foundry technology, crystal growth, coating and purification of materials, welding process, etc. Unlike the classical Stefan problem for pure metals, alloy solidification involves complex heat and mass transport phenomena. For most metal alloys, there could be three regions, namely, solid region, mushy zone (dendrite arms and interdendritic liquid) and liquid region in solidification process. Solidification of binary mixtures does not exhibit a distinct front separating solid and liquid phases. Instead, the solid is formed as a permeable, fluid saturated, crystal-line-like matrix. The structure and extent of this mushy region, depends on numerous factors, such as the specific boundary and initial conditions. During solidification, latent energy is released at the interfaces which separate the phases within the mushy region. The distribution of this energy therefore depends on the specific structure of the multiphase region. Latent energy released during solidification is transferred by conduction in the solid phase, as well as by the combined effects of conduction and convection in the liquid phase. To investigate the heat and mass transfer during the solidification process of an alloy, a few models have been proposed. They can be roughly classified into the continuum model and the volume-averaged model. Based on principles of classical mixture theory, Bennon & Incropera (1987) developed a continuum model for momentum, heat and species transport in the solidification process of a binary alloy. Voller et al. (1989) and Rappaz & Voller (1990) modified the continuum model by considering the solute distribution on microstructure, the so-called Scheil approach. Beckermann & Viskanta (1988) reported an experimental study on dendritic solidification of an ammonium chloride-water solution. A numerical simulation for the same physical configuration was also performed using a volumetric averaging technique. Subsequently, the volumetric averaging technique was systematically derived by Ganesan & Poirier (1990) and Ni & Beckermann (1991). Detailed discussions on microstructure formation and mathematical modelling of transport phenomenon during solidification of binary systems can be found in

the reviews of Rappaz (1989) and Viskanta (1990).
In the last few decades intensive studies have been made to model various problems, for example: to solve radiative transfer problem in triangular meshes, Feldheim & Lybaert (2004) used discrete transfer method (DTM can be see in the work of Lockwood & Shah (1981)), Galerkin finite element method was used by Wiwatanapataphee et al. (2004) and Tryggvason et al. (2005) to study the turbulent fluid flow and heat transfer problems in a domain with moving phase-change boundary and Dimova et al. (1998) also used Galerkin finite element method to solve nonlinear phenomena. Finite volume method for the calculation of solute transport in directional solidification has been studied and validated by Lan & Chen (1996). Finite element method to model the filling and solidification inside a permanent mold is performed by Shepel & Paolucci (2002). Three dimensional parallel simulation tool using a unstructured finite volume method with Jacobian-free Newton-Krylov solver, has been done by Knoll et al. (2001) for solidifying flow applications. Also arbitrary Lagrangian-Euler (ALE) formulation was develop by Bellet & Fachinotti (2004) to simulate casting processes, among others. One of the major challenges of heat transfer modelling of molten metal has been the phase change. To model such a phase change requires the strict imposition of boundary conditions. Normally, this could be achieved with a finite-element that is distorted to fit the interface. Since the solid-liquid phase boundaries are moving the use of level set methods are a recent trend (Sethian (1996)). However, both of these techniques are computationally expensive. The classical fixed mesh is computational less expensive but could not been able to maintain the correct boundary conditions. In this regard, Monteiro (1996) studied the application of the finite difference method to permanent mold casting using generalized curvilinear coordinates. A multi-block grid was applied to a complex geometry and the following boundary conditions: continuity condition to virtual interfaces and convective heat transfer to metal-mold and mold-environment interfaces. The reproduction of this simulation procedure using the finite volume method was made by Monteiro (2003). The agreement with experimental data was also good. Further developments of this work were made by Monteiro & Rouboa (2005) where more reliable initial conditions and two different kinds of boundary conditions were applied with an increase in agreement with the experimental data. In the present work we compare the finite difference and finite volume methods in terms of space discretization, boundary conditions definition, and results using a multi-block grid in combination with curvilinear coordinates. The multi-block grid technique allows artificially reducing the complexity of the geometry by breaking down the real domain into a number of subdomains with simpler geometry. However, this technique requires adapted solvers to a nine nodes computational cell instead of the five nodes computational cell used with cartesian coordinates for two dimensional cases. These developments are presented for the simple iterative methods Jacobi and Gauss-Seidel and also for the incomplete factorization method strongly implicit procedure.

2. Heat transfer and governing equations

Solidification modelling can be divided into three separate models, where each model is identified by the solution to a separate set of equations: *heat transfer modelling* which solves the energy equation; *fluid-flow modelling* which solves the continuity and momentum equations; and *free-surface modelling* which solves the surface boundary conditions. For a complete description of a casting solidification scenario, all these equations should be solved simultaneously, but under special circumstances they could be decoupled and modelled independently. This is the case for heat-transfer modelling, which has been widely used, and

its application has significantly improved casting quality (Swaminathan & Voller (1997)).

2.1 Mathematical model

The governing system equations is composed by the heat conservative equation, the boundary condition equations and the initial equation. In this section, differential equations of the heat conservative and adapted boundary conditions for the solidification phenomena will be presented.

2.1.1 Energy conservation equation

The energy conservation equation states that the rate of gain in energy per unit volume equals the energy gained by any source term, minus the energy lost by conduction, minus the rate of work done on the fluid by pressure and the viscous forces, per unit time. Assuming that: the fluid is isotropic and obeys Fourier's Law; the fluid is incompressible and obeys the continuity equation; the fluid conductivity is constant; viscous heating is negligible, and since the heat capacity of a liquid at constant volume is approximately equal to the heat capacity at constant pressure, then, the internal energy equation is reduced to the familiar heat equation, here shown in curvilinear coordinates (Monteiro et al. (2006), Monteiro & Rouboa (2005)). The governing differential equation for the solidification problem may be written in the following conservative form

$$\frac{\partial \left(\rho C_P \phi\right)}{\partial t} = \nabla \cdot \left(k \nabla \phi\right) + \dot{q}, \tag{1}$$

where $\frac{\partial(\rho C_P \phi)}{\partial t}$ represents the transient contribution to the conservative energy equation (ϕ temperature); $\nabla \cdot (k \nabla \phi)$ is the diffusive contribution to the energy equation and $\dot{q}$ represents the energy released during the phase change. The physical properties of the metal: the metal density ρ (kg/m^3), the heat capacity of constant pressure C_P (J/kg^oC) and the thermal conductivity k (W/m^oC) are considered to be constants analogously as done by Knoll et al. (2001), Monteiro (1996) and Shamsundar & Sparrow (1975).

The term $\dot{q}$ can be expressed as a function of effective solid (Monteiro (1996)), (*s solidus* or solidified metal) material fraction f_s, metal density ρ, and enthalpy variation during the phase change Δh_f called latent heat (Monteiro & Rouboa (2005), Monteiro et al. (2006)), by the following expression

$$\dot{q} = \frac{\partial \left(\rho \Delta h_f \, f_s\right)}{\partial t}. \tag{2}$$

One can also decompose f_s in the following way

$$\frac{\partial f_s}{\partial t} = \frac{\partial f_s}{\partial \phi} \frac{\partial \phi}{\partial t}. \tag{3}$$

Assuming that Δh_f is independent of temperature and the material is isotropic, one substitutes equations (2) and (3) in equation (1) and obtain

$$\frac{\partial \phi}{\partial t} \left(1 - \frac{\Delta h_f}{C_P} \frac{\partial f_s}{\partial \phi}\right) = a \left(\bigtriangledown^2 \phi\right), \tag{4}$$

where a is the thermal diffusivity which is equal to $a = \frac{k}{\rho C_p}$ (m^2/s).

The solid fraction can be determined, at each temperature, by the lever rule. When dealing

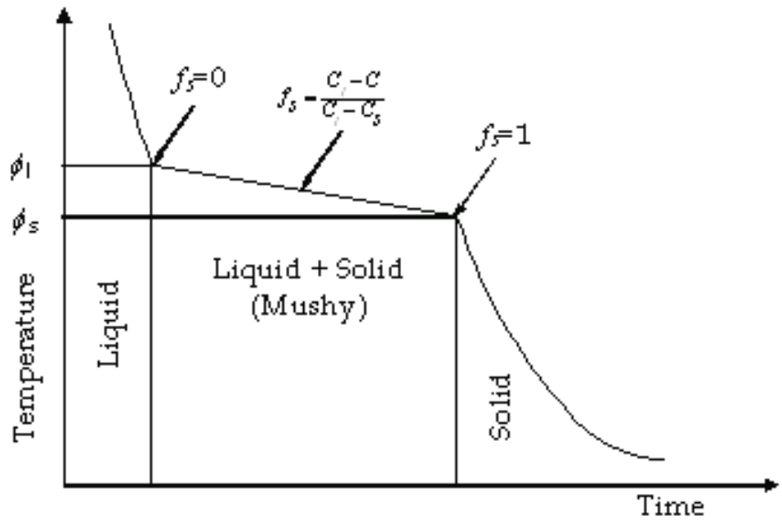

Fig. 1. Typical cooling diagram of alloys

with small temperature difference, a linear relationship between $f_s(\phi)$ and ϕ, is an acceptable approximation as shown in the Fig. 1. Thus, $\frac{\partial f_s}{\partial \phi}$ can be considered as constant. The constant ϕ_s is the solidus temperature, ϕ_l is the liquidus temperature and during the mushy phase the material fraction f_s is given by $f_s = \frac{C_l - C}{C_l - C_s}$, where C is the concentration, C_l and C_s are, respectively, the liquidus and solidus concentrations. This assumption allows the linearization of the source term of the energy equation.
One also uses the *curvilinear coordinates* which transforms the domain into rectangular and time independent. The calculation is given by a uniform mesh of squares in a two dimension, by the following transformation: $x_i = x_i(\xi_1, \xi_2)$, for $i = 1,2$, characterized by the Jacobian J

$$J = \det \left[\frac{\partial x_i}{\partial \xi_j} \right]_{i,j}. \tag{5}$$

Therefore,

$$\frac{\partial \phi}{\partial x_i} = \frac{\partial \phi}{\partial \xi_j} \frac{\partial \xi_j}{\partial x_i} = \frac{\partial \phi}{\partial \xi_j} \frac{\beta^{ij}}{J}, \tag{6}$$

where $\beta^{ij} = (-1)^{i+j} \det(J_{ij})$ represents the cofactor in the Jacobian J, and J_{ij} is the Jacobian matrix taking out the line i and column j. Substituting the equation (6) in equation (4) one obtains

$$J \frac{\partial \phi}{\partial t} \left(1 - \frac{\Delta h_f}{C_P} \frac{\partial f_s}{\partial \phi} \right) = a \frac{\partial}{\partial \xi_j} \left[\frac{1}{J} \left(\frac{\partial \phi}{\partial \xi_m} B^{mj} \right) \right], \tag{7}$$

where the coefficient B^{mj} are defined by

$$B^{mj} = \beta^{kj} \beta^{km} = \beta^{1j} \beta^{1m} + \beta^{2j} \beta^{2m}. \tag{8}$$

The coefficient B^{mj} becomes zero when the grid is orthogonal, therefore the use of these coefficients in the equation (7).
The second term of equation (7) can be expressed by

$$J\frac{\partial\phi}{\partial t}\left(1-\frac{\Delta h_f}{C_P}\frac{\partial f_s}{\partial\phi}\right) = C_1\frac{\partial\phi}{\partial\xi_1}+C_2\frac{\partial\phi}{\partial\xi_2}+C_{11}\frac{\partial^2\phi}{\partial\xi_1^2}+C_{12}\frac{\partial^2\phi}{\partial\xi_1\partial\xi_2}+C_{22}\frac{\partial^2\phi}{\partial\xi_2^2}, \quad (9)$$

where

$$C_1 = \frac{\partial J^{-1}}{\partial\xi_1}B^{11}+\frac{\partial J^{-1}}{\partial\xi_2}B^{12}+J^{-1}\left(\frac{\partial B^{11}}{\partial\xi_1}+\frac{\partial B^{12}}{\partial\xi_2}\right),$$

$$C_2 = \frac{\partial J^{-1}}{\partial\xi_1}B^{21}+\frac{\partial J^{-1}}{\partial\xi_2}B^{22}+J^{-1}\left(\frac{\partial B^{21}}{\partial\xi_1}+\frac{\partial B^{22}}{\partial\xi_2}\right),$$

$$C_{11}=J^{-1}B^{11}, \quad C_{12}=J^{-1}\left(B^{21}+B^{12}\right), \quad C_{22}=J^{-1}B^{22}.$$

2.1.2 Boundary conditions

In the present study heat transfer between cast part (p), mold (m) and environment (e) is investigated. The parameters of thermal behavior of the part/mold boundary govern the heat transfer, determining solidification progression. The heat flow through an interface will be the result of the combination of several modes of heat transfer. Furthermore, the value of the heat transfer coefficient varies with several factors. It is generally accepted that the heat transfer resistance at the interface originates from the imperfect contact or even separation of the cast part metal and the mold. It means a gap is formed between the casting and the mold during the casting (Wang & Matthys (2002), Lau et al. (1998)). Different possibilities must be considered for heat transfer conditions on the boundary:

i) Continuity condition

$$\left(\frac{\partial\phi}{\partial n}\right)_{m_1}=\left(\frac{\partial\phi}{\partial n}\right)_{m_2}, \qquad \phi_{m_1}=\phi_{m_2} \quad (10)$$

is considered for the boundaries within continuous contact materials m_1 and m_2 (Monteiro (1996)). This means that the heat flux is fully transferred from the material m_1 to material m_2 without heat lost. These two materials are represented as blocks in the next sections.

ii) For the interface between different kind of materials, convective heat transfer is considered

$$k_m\left(\frac{\partial\phi}{\partial n}\right)_m = h^*\left(\phi_p-\phi_m\right), \quad (11)$$

where ϕ_m is the mold temperature, ϕ_p is the cast part temperature, h^* is the convective heat transfer coefficient and k_m in the thermal conductivity of the mold.

iii) For the exterior boundary in contact with the environment we have convection and radiation. From the work of Shi & Guo (2004) one has a mixed convection-radiation boundary condition given by

$$k_m\left(\frac{\partial\phi}{\partial n}\right)_m = h_{cr}\left(\phi_m-\phi_e\right), \quad (12)$$

here ϕ_e is the environment temperature and the convection-radiation heat transfer h_{cr} is calculated explicitly as follows

$$h_{cr} = \left(h_c + \varepsilon_r \sigma_r \left(\phi_m^3 - \phi_e^3\right)\right),$$

where ε_r is emissivity of the material, σ_r the Stefan-Boltzmann constant and the convective heat transfer coefficient h_c was considered equal to $150 W/m^{2^o} C$ (see Monteiro (1996)).

The governing system equations is composed by the heat conservative equation, the boundary condition equations and the initial equation. Despite the continuous efforts made by numerous studies, analytical solutions of such phase change problems are still limited to a few idealized situations. This is mainly because of the moving boundaries (interfaces) among different phases, the locations of which are essentially unknown. A comprehensive review of existing exact solutions can be found in the work of Carslaw & Jaeger (1959). On the other hand, numerous approximate methods including heat balance integral (Goodman (1958)), moving heat source (Lightfoot (1929)), and perturbation (Pedroso & Domoto (1973)) have been proposed to simplify the problem.

3. Numerical solution method

In this section, the discretization of the energy conservation equation coupling with convective boundary conditions using finite difference (FD), finite volume (FV) methods is presented. Furthermore, the development of the classical simple iterative methods: Jacobi and Gauss-Seidel and also for the incomplete factorization method strongly implicit procedure (SIP) is introduced in order to be used with curvilinear coordinates systems in a two dimensional domain.

3.1 Finite volume and finite difference

The most used approaches to discretization of the energy conservation equation coupling with convective boundary conditions are finite difference, finite volume and finite element methods. Here we use only the finite volume and finite difference methods. For the time discretization one uses the Crank-Nicholson semi implicit method (Ferziger & Peric (1999)).

3.1.1 Finite volume method

In the case of the FV method, two levels of approximation are needed for surface integrals: the integral is approximated in terms of the variables values at one location on the cell face, the midpoint point rule was used in this task; the cell face values are approximated in terms of the nodal values (control volume (CV) centers), the linear interpolation was used in this task. Fig. 2 shows the computational domain for FV discretization methods, using a geographical notation: E (east), N (north), S (south), W (west), NE (northeast), NW (northwest), SE (southeast), SW (southwest).

The volume integrals were approximated by a second-order approximation replacing the volume integral by the product of the mean value and the CV volume (Versteeg & Malalasekera (1995)). In this case, follows the expression for the first derivative

$$\int_V \frac{\partial \phi}{\partial \xi_i} dV = \frac{\phi_E - \phi_W}{2\Delta\xi_i} \Delta V, \tag{13}$$

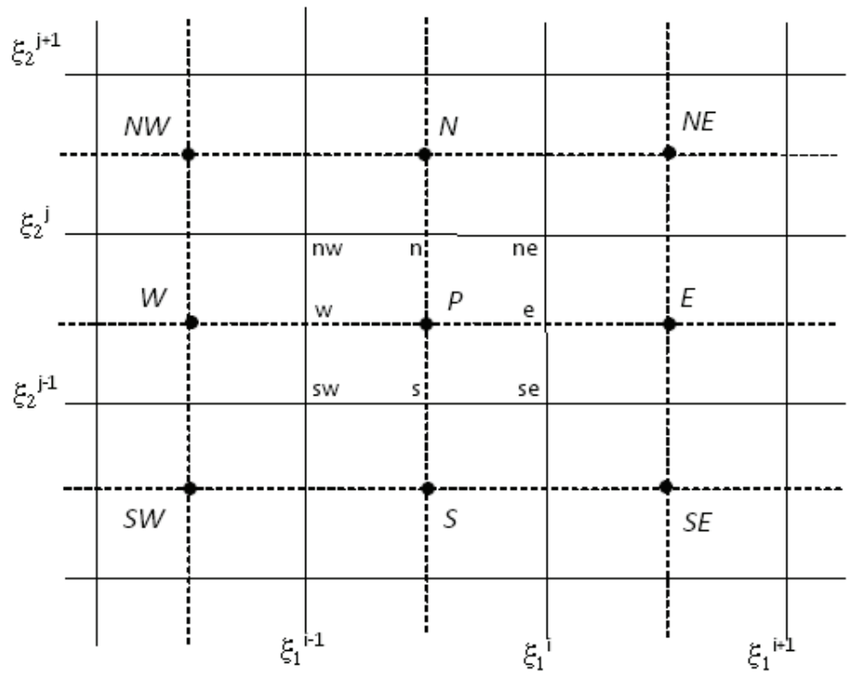

Fig. 2. Boundary condition treatment for finite volume method

and the second order derivatives are approximated as follows

$$\int_V \frac{\partial^2 \phi}{\partial \xi_i^2} dV = \int_S \frac{\partial \phi}{\partial \xi_i} \cdot \hat{n} dS = \left(\frac{\partial \phi}{\partial \xi_i}\right)_e S_e - \left(\frac{\partial \phi}{\partial \xi_i}\right)_w S_w, \tag{14}$$

$$\int_V \frac{\partial^2 \phi}{\partial \xi_i \partial \xi_j} dV = \int_V \frac{\partial}{\partial \xi_i}\left(\frac{\partial \phi}{\partial \xi_j}\right) dV = \frac{\left(\frac{\partial \phi}{\partial \xi_j}\right)_n S_n - \left(\frac{\partial \phi}{\partial \xi_j}\right)_s S_s}{\Delta \xi_i}. \tag{15}$$

Therefore, one can rewrite equation (9) as follows

$$\begin{aligned} & J\left(1 - \frac{\Delta h_f}{C_P}\frac{\partial f_s}{\partial \phi}\right)\left(\frac{\phi^{n+1} - \phi^n}{\triangle t}\right) \triangle V \\ = \; & \frac{1}{2}\left[\left(C_1 \frac{\partial \phi}{\partial \xi_1} + C_2 \frac{\partial \phi}{\partial \xi_2} + C_{11} \frac{\partial^2 \phi}{\partial \xi_1^2} + C_{12} \frac{\partial^2 \phi}{\partial \xi_1 \partial \xi_2} + C_{22} \frac{\partial^2 \phi}{\partial \xi_2^2}\right)^{n+1}\right. \\ + \; & \left.\left(C_1 \frac{\partial \phi}{\partial \xi_1} + C_2 \frac{\partial \phi}{\partial \xi_2} + C_{11} \frac{\partial^2 \phi}{\partial \xi_1^2} + C_{12} \frac{\partial^2 \phi}{\partial \xi_1 \partial \xi_2} + C_{22} \frac{\partial^2 \phi}{\partial \xi_2^2}\right)^{n}\right]. \end{aligned} \tag{16}$$

The discretization of the boundary condition derivatives are made by one side differences. The temperature value on each interface is computed considering the East surface interface of a general block 1 and the West surface interface a general block 2. One can see in Fig. 2 the boundary condition for FV methods, where P represents the node where the partial differential equation value is calculated.

The discretization of equation (10) allows us to obtain an explicit expression to determine the temperature on virtual interfaces, which is valid for FV discretization method and is given by

$$\phi_{m_1}(n,j) = \phi_{m_2}(0,j) = \frac{1}{2}\left(\phi_{m_1}(n-1,j) + \phi_{m_2}(1,j)\right). \tag{17}$$

The interface metal-mold using the FV method, is computed by

$$\phi_{m_1}(n,j) = \phi_{m_1}(n-1,j) + \frac{h_{m_1}}{2k\triangle\xi_1}\left(\phi^{old}_{m_1}(n,j) - \phi^{old}_{m_2}(0,j)\right), \tag{18}$$

$$\phi_{m_2}(0,j) = \phi_{m_2}(1,j) + \frac{h_{m_1}}{2k_m\triangle\xi_1}\left(\phi^{old}_{m_2}(0,j) - \phi^{old}_{m_1}(n,j)\right), \tag{19}$$

where $\phi^{old}_{m_l}$, for $l = 1,2$, is the previous iteration. For the interface mold-environment we have

$$\phi_{m_1}(n,j) = \phi_{m_1}(n-1,j) + \frac{h_{cr}}{2k_m\triangle\xi_1}\left(\phi_e - \phi^{old}_{m_2}(0,j)\right). \tag{20}$$

3.1.2 Finite difference method

Using a geographical notation, Fig. 3 shows the computational domain for FD discretization method.

In this case, the derivatives are approximated using the central difference scheme as follows

$$\frac{\partial\phi}{\partial\xi_i} = \frac{\phi_E - \phi_W}{2\Delta\xi_i}, \tag{21}$$

and the second order derivatives are approximated as follows

$$\frac{\partial^2\phi}{\partial\xi_i^2} = \frac{\phi_E - 2\phi_P - \phi_W}{2\Delta\xi_i^2}, \tag{22}$$

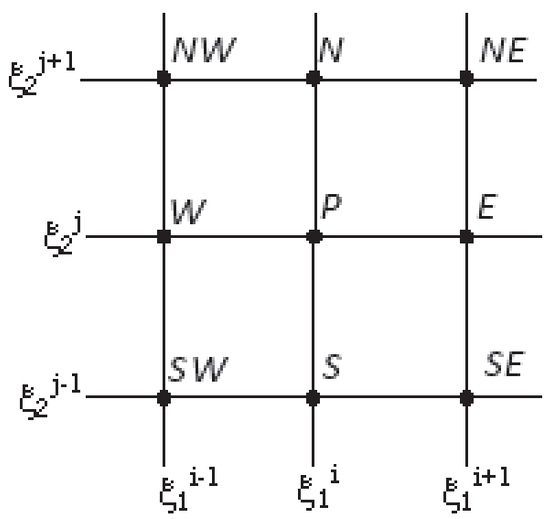

Fig. 3. Boundary condition treatment for finite difference method

$$\frac{\partial^2\phi}{\partial\xi_i\partial\xi_j} = \frac{\phi_{NE}-\phi_{SE}-\phi_{NW}+\phi_{SW}}{4\Delta\xi_i\Delta\xi_j}. \tag{23}$$

Therefore, one can rewrite equation (9) as follows

$$\begin{aligned} & J\left(1-\frac{\Delta h_f}{C_P}\frac{\partial f_s}{\partial\phi}\right)\left(\frac{\phi^{n-1}-\phi^n}{\triangle t}\right) \\ = \; & \frac{1}{2}\left[\left(C_1\frac{\partial\phi}{\partial\xi_1}+C_2\frac{\partial\phi}{\partial\xi_2}+C_{11}\frac{\partial^2\phi}{\partial\xi_1^2}+C_{12}\frac{\partial^2\phi}{\partial\xi_1\partial\xi_2}+C_{22}\frac{\partial^2\phi}{\partial\xi_2^2}\right)^{n+1}\right. \\ + \; & \left.\left(C_1\frac{\partial\phi}{\partial\xi_1}+C_2\frac{\partial\phi}{\partial\xi_2}+C_{11}\frac{\partial^2\phi}{\partial\xi_1^2}+C_{12}\frac{\partial^2\phi}{\partial\xi_1\partial\xi_2}+C_{22}\frac{\partial^2\phi}{\partial\xi_2^2}\right)^{n}\right]. \end{aligned} \tag{24}$$

The discretization of the boundary condition derivatives are made by one side differences. The temperature value on each interface is computed considering the East surface interface of a general block 1 and the West surface interface a general block 2.
The discretization of equation (10) allows us to obtain an explicit expression to determine the temperature on virtual interfaces, which is valid for both FV and FD discretization methods and is given by

$$\phi_{m_1}(n,j)=\phi_{m_2}(0,j)=\frac{1}{2}\left(\phi_{m_1}(n-1,j)+\phi_{m_2}(1,j)\right). \tag{25}$$

The interface metal-mold using the FD method, is computed by

$$\phi_{m_1}(n,j) = \phi_{m_1}(n-1,j)+\frac{h_{m_1}\triangle\xi_2}{k}\left(\phi_{m_1}^{old}(n,j)-\phi_{m_2}^{old}(0,j)\right), \tag{26}$$

$$\phi_{m_2}(0,j) = \phi_{m_2}(1,j)+\frac{h_{m_1}\triangle\xi_2}{k_m}\left(\phi_{m_2}^{old}(0,j)-\phi_{m_1}^{old}(n,j)\right), \tag{27}$$

where the first equation is related to the metal block and the second is related to the mold block. For the interface mold-environment we have

$$\phi_{m_1}(n,j) = \phi_{m_1}(n-1,j)+\frac{h_{cr}\triangle\xi_2}{k_m}\left(\phi_e-\phi_{m_2}^{old}(0,j)\right). \tag{28}$$

3.2 Jacobi, Gauss-Seidel and Stone's methods

Here, the development of the classical solvers (*Jacobi*,*Gauss-Seidel*) and *Stone's* solver also known as *strongly implicit procedure (SIP)* is presented in the way to be used with curvilinear coordinates in two dimensional domains. The aim is to apply these methods to non-orthogonal grid.

From the FV or FD discretisation procedure one obtains a linear system of the form

$$A\Theta = Q, \tag{29}$$

where A is a sparse matrix, Θ the variable in computation and Q a vector of independent terms (see e.g. Ferziger & Peric (1999), Pina (1995), Tannehill (1997)). The coefficient matrix will typically take on a hepta diagonal structure, with the non-zero components occupying only seven diagonals of the matrix. For a two dimensional partial differential equations there will

be only five diagonals which are non-zero. For unstructured meshes, the coefficient matrix will also take a diagonal structure, with the non-zero components occupying nine diagonals of the matrix for two dimensional. This regular structure enables a considerable reduction in memory use and the number of operations performed.
The structure of the matrix A depends on the ordering of the variables in the vector Θ. As in the work of Ferziger & Peric (1999), one orders the entries in the vector Θ starting at the southwest corner of the domain, proceeding northwards along each grid and then eastward across the domain. The algebraic equation for a particular control volume in a two dimensional domain, see Fig. 2, using curvilinear coordinates, is of the form

$$A_P\Theta_p + \sum_{nb} A_{np}\Theta_{np} = Q_p, \tag{30}$$

where P represents the node where the partial differential equation value is calculated and the index nb represents the neighborhood nodes involved in the approach. Using a geographical notation: E (east), N (north), S (south), W (west), NE (northeast), NW (northwest), SE (southeast), SW (southwest), the sum is extended in the following form

$$\begin{aligned}\sum_{nb} A_{np}\Theta_{np} &= A_E\Theta_E + A_W\Theta_W + A_N\Theta_N + A_S\Theta_S \\ &+ A_{NE}\Theta_{NE} + A_{SE}\Theta_{SE} + A_{NW}\Theta_{NW} + A_{SW}\Theta_{SW}.\end{aligned} \tag{31}$$

The properties of the linear system (29) are important when setting up an iteration method for its solutions. Let us present some of the classical iteration methods modified to the problem treated here.

3.2.1 Jacobi's method

In the Jacobi method the resulting equations from the discretisation process are determined separately. Equation (31) is modified assuming the following form

$$\Theta_P = (A_P)^{-1}\left(Q_P - \sum_{nb\neq P} A_{nb}\Theta_{nb}\right). \tag{32}$$

Having the following iterative method defined as

$$\Theta_P^{(k)} = (A_P)^{-1}\left(Q_P - \sum_{nb\neq P} A_{nb}\Theta_{nb}^{(k-1)}\right), \tag{33}$$

where all the terms of the equation (33) are related to the last iteration release. In the Jacobi method the used values are of the previous iteration in the way to get the values of the following iteration. However, when we are calculating the new, the actual value is already known.

3.2.2 Gauss-Seidel's method

The Gauss-Seidel method, in contrast with the Jacobi method, uses the actual values in detriment of the ones of the previous iteration (see Pina (1995), Norris (2001)). This idea leads to the following modification of equation (33)

$$\Theta_P^{(k)} = (A_P)^{-1}\left(Q_P - \sum_{nb\in\{SW,W,NE,S\}} A_{nb}\Theta_{nb}^{(k)} - \sum_{nb\in\{N,NE,E,SE\}} A_{nb}\Theta_{nb}^{(k-1)}\right).$$

Usually, this method converges faster than the Jacobi method.

3.2.3 Stone's method

The *strongly implicit procedure (SIP)*, also known as the Stone's method (Stone (1968)), is known for solving the system of algebraic equations that arises, for instance, in the finite differences or finite analytic description of field problems (Schneider & Zedan (1981)). This procedure was also used in multi-phase fluid flow and heat transfer problems (Peric (1987)). The SIP solver is an advanced version of the incomplete LU decomposition

$$M = LU,$$

where M is the iterative matrix, L (lower triangular) and U (upper triangular) matrices. The matrix M is given by the splitting of the matrix A in the form $M = A + N$, such that M is a good approximation to A.

This method will be described for a nine-point computational cell (see Fig. 2). The L (lower) and U (upper) matrices have non-zero elements only on diagonals on which A has non-zero elements. The product of lower and upper triangular matrices with these structures has more non-zero diagonals than A.

For the nine-point computational cell there are four diagonals (corresponding to nodes NN (north-north), NNW (nor-norwest) , SS (south-south), SSE (sud-southeast), SS (south-south)) as can be seen in Fig. 4.

The nine sets of elements (five in L and four in U) are determined using the rules of multiplication matrix as follows

$$\begin{aligned}
M_{SW} &= L_{SW} \\
M_{W} &= L_{SW}U_{N} + L_{W} \\
M_{NW} &= L_{W}U_{N} + L_{NW} \\
M_{NNW} &= L_{NW}U_{N} \\
M_{SS} &= L_{SW}U_{SE} \\
M_{S} &= L_{SW}U_{E} + L_{W}U_{SE} + L_{S} \\
M_{P} &= L_{SW}U_{NE} + L_{W}U_{E} + L_{NW}U_{SE} + L_{S}U_{N} + L_{P} \\
M_{N} &= L_{W}U_{NE} + L_{NW}U_{E} + L_{P}U_{N} \\
M_{NN} &= L_{NW}U_{NE} \\
M_{SSE} &= L_{S}U_{SE} \\
M_{SE} &= L_{S}U_{E} + L_{P}U_{E} \\
M_{E} &= L_{S}U_{NE} + L_{P}U_{E} \\
M_{NE} &= L_{P}U_{NE},
\end{aligned} \tag{34}$$

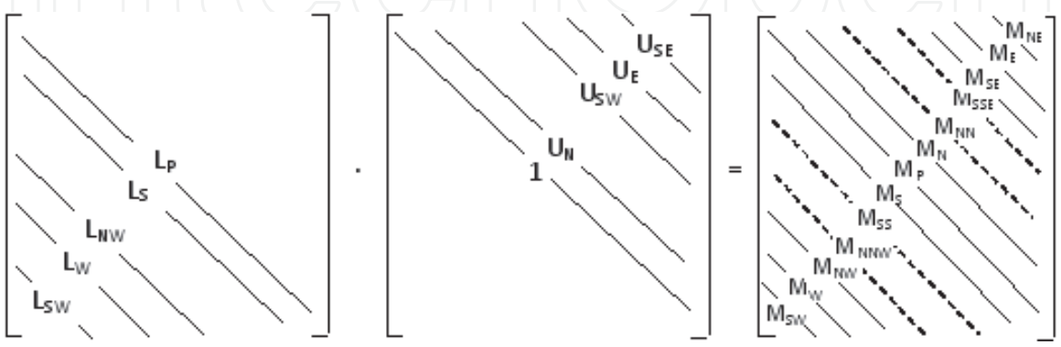

Fig. 4. Schematic presentation of the matrices L (Lower), U (Upper) and the product matrix M; diagonals of M not found in A are shown by dashed lines

we consider M_X to be the matrix with only the diagonal M_X non-zero as for L_X and U_X.
We wish to select matrices L and U, in order to obtain M as a good approximation to A and consequently has a faster convergence of the method. For this reason the matrix N must contain, at least, the four diagonals of the matrix M which correspond to zero diagonals of A. Furthermore, N has to have non-zero elements only on these diagonals. Therefore, the other diagonals of matrix M has the corresponding diagonals of A.
Stone (1968) recognized that convergence can be improved by allowing matrix N to have non-zero elements on the diagonal corresponding to all thirteen non-zero diagonals of LU.
Considering the vector $M\Theta$, the method can be easily derived

$$\begin{aligned}(M\Theta)_P &= M_P\Theta_P + M_S\Theta_S + M_N\Theta_N + M_E\Theta_E + M_W\Theta_W \\ &+ M_{NE}\Theta_{NE} + M_{NW}\Theta_{NW} + M_{SE}\Theta_{SE} + M_{SW}\Theta_{SW} \\ &+ M_{NNW}\Theta_{NNW} + M_{SSE}\Theta_{SSE} + M_{NN}\Theta_{NN} + M_{SS}\Theta_{SS}.\end{aligned} \tag{35}$$

Each term in this equation corresponds to a diagonal of $M = LU$. The matrix N must contain the four last terms which are the extra diagonals of M, and the elements on the remaining diagonals, are chosen so that $N\Theta \approx 0$, this is,

$$\begin{aligned}&N_P\Theta_P + N_S\Theta_S + N_N\Theta_N + N_E\Theta_E + N_W\Theta_W \\ &+N_{NE}\Theta_{NE} + N_{NW}\Theta_{NW} + N_{SE}\Theta_{SE} + N_{SW}\Theta_{SW} \\ &+N_{NNW}\Theta_{NNW} + N_{SSE}\Theta_{SSE} + N_{NN}\Theta_{NN} + N_{SS}\Theta_{SS} \approx 0.\end{aligned} \tag{36}$$

This requires that the contribution of the four extra terms, in the above equation, have to be nearly canceled by the contribution of other diagonals, i.e., equation (35) should be reduce to the following expression

$$\begin{aligned}&M_{NNW}\left(\Theta_{NNW} - \Theta^*_{NNW}\right) + M_{SSE}\left(\Theta_{SSE} - \Theta^*_{SSE}\right) \\ &+M_{NN}\left(\Theta_{NN} - \Theta^*_{NN}\right) + M_{SS}\left(\Theta_{SS} - \Theta^*_{SS}\right) \approx 0,\end{aligned} \tag{37}$$

where $\Theta^*_{NNW}, \Theta^*_{SSE}, \Theta^*_{NN}, \Theta^*_{SS}$ are approximations of $\Theta_{NNW}, \Theta_{SSE}, \Theta_{NN}, \Theta_{SS}$, respectively.
Rouboa et al. (2009) considered the following possible approximation

$$\begin{aligned}\Theta^*_{NNW} &= \alpha\left(\Theta_{NW} + \Theta_N + \Theta_W - 2\Theta_P\right) \\ \Theta^*_{NN} &= \alpha\left(\Theta_N + \Theta_{NE} + \Theta_{NW} - 2\Theta_P\right) \\ \Theta^*_{SS} &= \alpha\left(\Theta_S + \Theta_{SW} + \Theta_{SE} - 2\Theta_P\right) \\ \Theta^*_{SSE} &= \alpha\left(\Theta_S + \Theta_{SE} + \Theta_E - 2\Theta_P\right),\end{aligned} \tag{38}$$

where $\alpha < 1$ for stability reasons.
Substituting (38) into equation (37) and comparing the result with equation (36), we obtain all elements of matrix N as linear combinations of M_{NNW}, M_{SSE}, M_{NN} and M_{SS}. Elements of the matrix M can be set equal to the sum of matrix elements of A and N.
The resulting equations are not only sufficient to determine all of the elements of the matrix L and U, but they can be solved in sequential order beginning at the southwest corner of the grid

$$L^{ij}_{SW} = \frac{A^{ij}_{SW}}{1 + \alpha U^{(i-1),(j-1)}_{SE}}$$

$$
\begin{aligned}
L_W^{ij} &= A_W^{ij} + L_{SW}^{ij} U_N^{ij} - \alpha L_{NW}^{ij} U_N^{(i-1),(j+1)} \\
L_{NW}^{ij} &= \frac{A_S^{ij} - L_W^{ij} U_N^{i-1,j}}{1 + \alpha \left(U_N^{(i-1),(j+1)} + U_{NE}^{i-1,j+1} \right)} \\
L_S^{ij} &= \frac{A_S^{ij} - L_{SW}^{ij} U_E^{i-1,j-1} - L_W^{ij} U_{SE}^{i-1,j} - \alpha L_{SW}^{ij} U_{SE}^{i-1,j-1}}{1 + \alpha U_{SE}^{i,j-1}} \\
L_P^{ij} &= A_P^{ij} - L_{SW}^{ij} U_{NE}^{i-1,j-1} - L_W^{ij} U_E^{i-1,j} - L_{NW}^{ij} U_{SE}^{i-1,j+1} - L_S^{ij} U_N^{i,j-1} \\
&+ 2\alpha \left(L_{SW}^{ij} U_{SE}^{i-1,j-1} + L_S^{ij} U_{SE}^{i-1,j+1} + L_{NW}^{ij} \left(U_{NE}^{i-1,j+1} + U_N^{i-1,j+1} \right) \right) \\
U_N^{ij} &= \frac{A_N^{ij} - L_W^{ij} U_{NE}^{i-1,j} - L_{NW}^{ij} U_E^{i-1,j+1} - \alpha L_{NW}^{ij} U_{NE}^{i-1,j+1}}{L_P^{ij} + \alpha L_{NW}^{ij}} \\
U_{SE}^{ij} &= \frac{A_{SE}^{ij} - L_S^{ij} U_E^{i,j-1}}{L_P^{ij} + \alpha \left(L_{SW}^{ij} - L_S^{ij} \right)} \\
U_E^{ij} &= \frac{A_E^{ij} - L_S^{ij} U_{NE}^{i,j-1} - \alpha L_S^{ij} U_{SE}^{i,j-1}}{L_P^{ij}} \\
U_{NE}^{ij} &= \frac{A_{NE}^{ij}}{L_P^{ij} + \alpha L_{NW}^{ij}}.
\end{aligned}
\tag{39}
$$

One considers that any matrix element that carries the index of a boundary node is zero. The equation system using this approximation is solved by iteration. The updated residual is calculated by the following equation

$$LU\delta^{n+1} = \rho^n.$$

The multiplication of the above equation by L^{-1} leads to

$$\delta^{n+1} = \quad L^{-1}\rho^n =: \quad R^n \tag{40}$$

where R is computed by

$$R^{ij} = \frac{\rho^{ij} - L_{SW}^{ij} R^{i-1,j-1} - L_S^{ij} R^{i,j-1} - L_{NW}^{ij} R^{i-1,j+1} - L_W^{ij} R^{i-1,j}}{L_P^{ij}}. \tag{41}$$

When the computation of R is complete, we need to solve equation (40) using

$$\delta^{ij} = R^{ij} - U_N^{ij} \delta^{i,j+1} - U_{NE}^{ij} \delta^{i+1,j+1} + U_E^{ij} \delta^{i+1,j} + U_{SE}^{ij} \delta^{i+1,j-1}, \tag{42}$$

in order of decreasing the i,j indexes.

4. Numerical applications

The aim of these present experiments is to validate the developed numerical code. We start by developing the classical solvers (Jacobi, Gauss-Seidel) and Stone method in order to use them with curvilinear coordinates systems in two dimensional domains. Furthermore, we compare the finite volume and finite difference methods in terms of space discretization, boundary conditions definition and results using a multi-block grid in combination with curvilinear coordinates.

The numerical simulation was carried out on a two dimensional domain constituted by the cross-section defined by the middle plane of the test part. In Fig. 5 the $D1$ domain is constituted by the cross-section of the part including the filling channel, the $D2$ domain is constituted by the cross-section of the inferior part of the mold, $D3$ and $D4$ correspond to superior part of the mold and both domains are fixed to each other.

Grid generation was carried out by bilinear interpolation (Thompson et al. (1985)) and each domain was subdivided in simpler subdomains, see Fig. 6.

The use of curvilinear formulation in conjunction with a multi-block grid could be an excellent method to test every kind of curvilinear link of piping in a single simulation. The part (domain $D1$) is filled in with the aluminium alloy ($Al12Si$) cast in a grey cast iron mold (domains $D2$, $D3$ and $D4$). The physical characteristics of the materials involved in the numerical simulation are shown in Table 1 (Monteiro (1996), Sciama & Visconte (1987)).

Property	Metalic alloy AI 12Si	Mold Grey cast-iron
Density (kg/m^3)	2670	7230
Thermal conductivity ($W/m^{\circ}C$)	185	38
Thermal heat capacity ($J/kg^{\circ}C$)	1260	750
Latent heat (kJ/kg)	395	$\cdots$
Liquidus temperature ($^{\circ}C$)	585	$\cdots$
Solidus temperature ($^{\circ}C$)	575	$\cdots$

Table 1. Physical properties

The liquidus and solidus temperatures were experimentally determined by a 50 KV high frequency induction furnace to melt the aluminium/silicon alloy used. K type thermocouples, constituted by the pair 5%Al Ni and 10%Cr-Ni with a total diameter of 1 mm, were used in the temperature measurements. A data acquisition board connected to a microcomputer was used to temperature recording. This board is responsible for the digitalization of the analogical signal produced by the thermocouples. The tested alloy is composed by aluminium with 12% of silicon (Al 12Si). The obtained cooling curve is represented in Fig. 7, from which is possible to determine that the liquidus temperature is 585^0C and the solidus temperature is 575^0C.

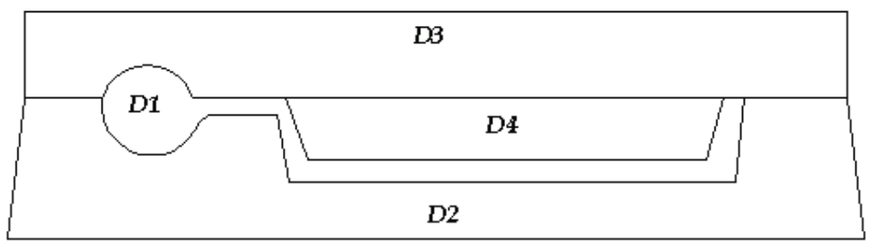

Fig. 5. Cross section of the mold/part set

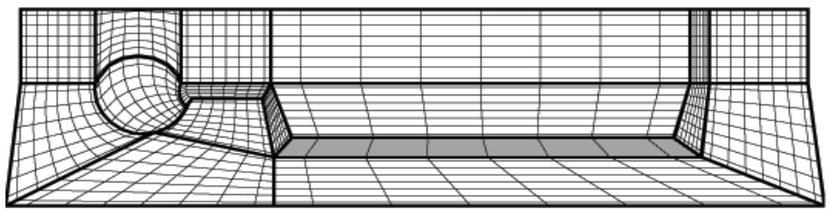

Fig. 6. Representation of the mesh used to discretize each of the subdomains

Fig. 8 shows the cross section of the studied domain and thermocouples locations. Due to the high temperature it was difficult to obtain stable values by thermocouples.
The environment temperature was considered to be constant, at 20^0C. During the filling of the mold by a gravity-fed system a significant volume of metal may solidify before the end of the process. To prevent the filling from being interrupted by premature solidification, the metal is usually cast into a hot mold. During the solidification process the initial temperature of the mold is considered uniform, as assumed in the previous works of Radovic & Lalovic (2005), Santos et al. (2003) and Shi & Guo (2004). For this reason the initial temperature field in the mold, considered uniform, was set to 300^0C. The initial temperature field in the part, considered also uniform, was set to 585^0C (liquidus temperature). The end of phase change is determined by the solidus temperature. The mold was divided into 17 polygons, Fig. 9 (Monteiro et al. (2006), Monteiro & Rouboa (2005)).
This phenomenon was applied on the outer wall of the mold. The convective heat transfer phenomena was adapted as boundary conditions between the following blocks

- block 1 with block 7, block 10, block 11, block 12;
- block 2 with block 7 and block 13;
- block 3 with block 7 and block 6;
- block 4 with block 6 and block 9;

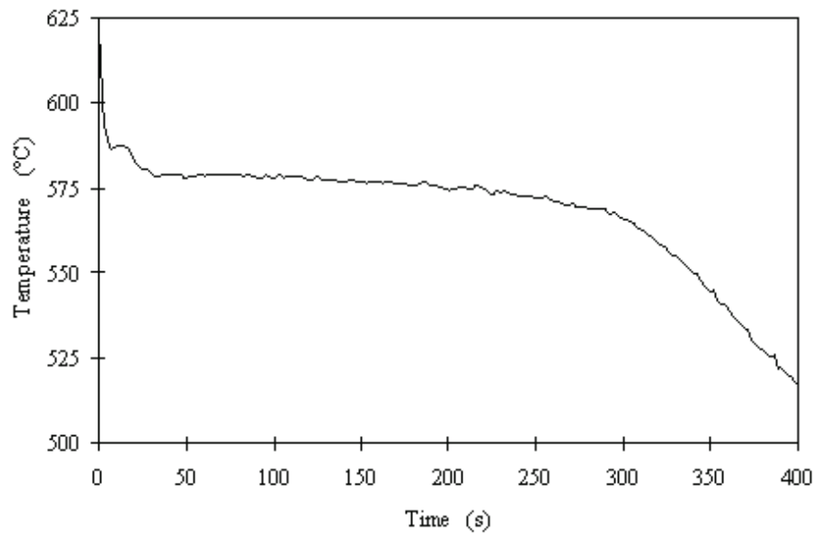

Fig. 7. Temperature profile during solidification of Al 12Si

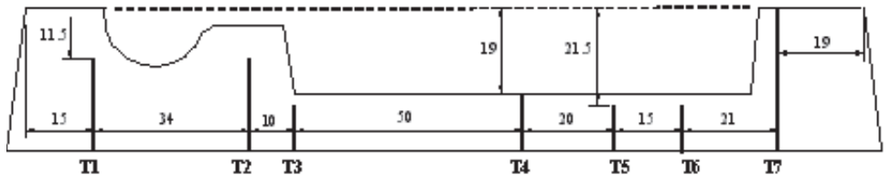

Fig. 8. Thermocouples (T1–T7) location (in mm) on the mold crosss-section

- block 5 with block 6 and block 8.

The convective heat transfer coefficients in Table 2 were determined using the inverse heat conduction problem of Beck (1970), which the basic principle is to assume that the heat flux is a constant on a linear function of time within a given time interval. The whole description of this technique can be found in the work of Lau et al. (1998). The definition of all coordinate

Interface	Convective heat transfer coefficient $[W/m^2\,^0C]$
Cast part/mold	$h_i = 2500$
Block 8/16	$h_i = 500$
Block 11/17	$h_i = 500$
Block 6/14	$h_i = 600$
Mold/environment	$h_i = 150$

Table 2. Convective heat transfer coefficients

lines in the interior of the domain is made by bilinear interpolation of the nodal position defined in the boundaries resulting in the grid showed in Fig. 6.
The physical characteristics of the material involved in the numerical simulation are shown in Table 1.

4.1 Performance of adapted solvers

In this study we adapt the simples iterative methods: Jacobi, Gauss-Seidel and the incomplete factorization method strongly implicit procedure (SIP) to generalized curvilinear coordinates and apply them to a complex geometry through the multi-block grid technique.
Since the analysis was made for each block, only some relevant block will be discussed further.

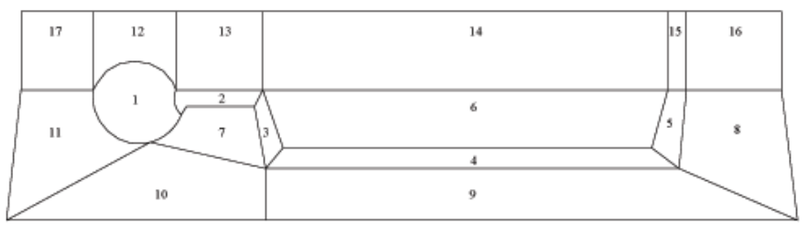

Fig. 9. Geometry division into 17 blocks

Subdomain	SIP		Gauss-Seidel		Jacobi	
Block	Iteration	Residue	Iteration	Residue	Iteration	Residue
1	1000	1.99×10^{-3}	1000	1.51	1000	1.51
2	2	8.90×10^{-4}	1000	0.46	1000	0.48
3	1000	1.05×10^{-3}	1000	0.33	1000	0.33
4	2	8.64×10^{-4}	1000	2.28	1000	2.28
5	2	9.18×10^{-4}	1000	0.53	1000	0.52
6	2	1.66×10^{-4}	1000	3.31	1000	3.32
7	2	1.54×10^{-4}	1000	0.57	1000	0.59
8	2	4.57×10^{-4}	1000	1.73	1000	1.65
9	2	6.41×10^{-5}	1000	1.66	1000	1.78
10	1000	1.91×10^{-3}	1000	1.59	1000	1.66
11	2	1.21×10^{-4}	1000	1.15	1000	1.27
12	2	4.44×10^{-5}	1000	0.34	1000	0.34
13	2	2.46×10^{-4}	1000	0.90	1000	1.05
14	1000	6.19×10^{-3}	1000	5.47	1000	5.36
15	2	2.85×10^{-4}	1000	0.25	1000	0.25
16	1000	3.07×10^{-3}	1000	0.78	1000	0.77
17	1000	1.31×10^{-3}	1000	0.37	1000	0.38

Table 3. Iterative performance

Consider Fig. 9, the block 1 which is the most complicated geometrical structure. After 1000 iterations it is observed, in Table 3, that the SIP method has better residual in comparison with the others two classical solvers.
For block 14 the same conclusion can be made after 1000 iterations, even though the regularity of its geometry and simplicity of its boundaries conditions. In fact, this block is submitted to natural convection on the top and conduction limit on the other three sides.
The block 7, that has more contact to the shape of the mold, converges after only 2 iterations for SIP solver. For the others cited solvers no convergence has been shown after 1000 iterations.
The block 9, presents the best residual result for the SIP solver, in relation to all block. Furthermore, its has a better residual result for the SIP methods only for 2 iterations compared to 1000 iteration made for the Jacobi and Gauss-Seidel methods.

4.1.1 Concluding remarks on numerical solvers

Adaptations of simple iterative methods (Jacobi and Gauss-Seidel) and the incomplete factorization method strongly implicit procedure (SIP) to generalized curvilinear coordinates was presented and its applicability in complex geometries through the multi-block grid technique was performed.
The complexity of the geometry, results showed that Jacobi and Gauss-Seidel solvers are not suitable. However, SIP method continues to have a reasonable performance. In conclusion strongly implicit procedure method, when combined with generalized curvilinear coordinates and multi-block grid technique, can be used in complex geometry problems when high precision results are not required.

4.2 Performance of finite differences and finite volume methods

The most used approaches to discretization of the energy conservation equation coupling with convective boundary conditions are finite difference, finite volume and finite element methods. For finer grid mesh, these methods yields the same approximately solution (Ferziger & Peric (1999), Versteeg & Malalasekera (1995)). Here we compare the FV and FD methods in terms of space discretization, boundary conditions definition and results using a multi-block grid in combination with curvilinear coordinates.

In this study the FV method is programmed using a multi-block grid applied in the case of heat transfer phenomena during solidification. Fig. 9 shows subdomains (blocks) of casting (block 1 to 5) and mold (block 6 to 17). The multi-block grid is generated by bilinear interpolation (Thompson et al. (1985)) with increased concentration of cells near the geometrical singularities where the thermal gradients are expected to be higher.

Due to the use of generalized curvilinear coordinates the calculations in each bock could be performed in a fixed square. Fig. 2 and Fig. 3 shows the computational domain for the FV and FD methods, respectively. In the FV method the domain is divided into a finite number of control volumes, which in opposite to the FD method defines the control volume limit and not the computational nodes.

4.2.1 Results and discussion

In this study, an analysis of heat transfer for the casting process in two dimensions was made for the nonlinear case during solidification taking into account the phase change. The time step used was 10^{-3} seconds. The result of the heat transfer is shown in two dimensions, as well as the cooling curves in different points in the cast metal and mold. The final step consists in solving the problem of heat transfer of the mold - cast metal system, using linearized equation (9) and controlled by the convergence criteria (10^{-5} for temperature). The SIP solver of Stone (1968) was used in this task. Numerical results calculated using FD and FV discretization methods were overlapped with experimental values, measured by the thermocouples $T1$, $T2$, $T3$, $T4$, $T5$, $T6$ and $T7$, shown in Fig. 10.

4.3 Concluding remarks

A multi-block grid generated by bilinear interpolation was successfully applied in combination with a generalized curvilinear coordinates system to a complex geometry in a casting solidification scenario. To model the phase change a simplified two dimensional mathematical model was used based on the energy differential equation. Two discretization methods: finite differences and finite volume were applied in order to determine, by comparison with experimental measurements, which works better in these conditions. For this reason a coarse grid was used. A good agreement between both discretization methods was obtained with a slight advantage for the finite volume method. This could be explained due to the use of more information by the finite volume method to compute each temperature value than the finite differences method. The multi-block grid in combination with a generalized curvilinear coordinates system has considerably advantages such as:

- better capacity to describe the contours through a lesser number of elements, which considerably reduces the computational time;
- any physical feature of the cast part or mold can be straightforwardly defined and obtained in a specific zone of the domain;
- the difficulty of the several virtual interfaces created by the geometry division are easily overcome by the continuity condition;

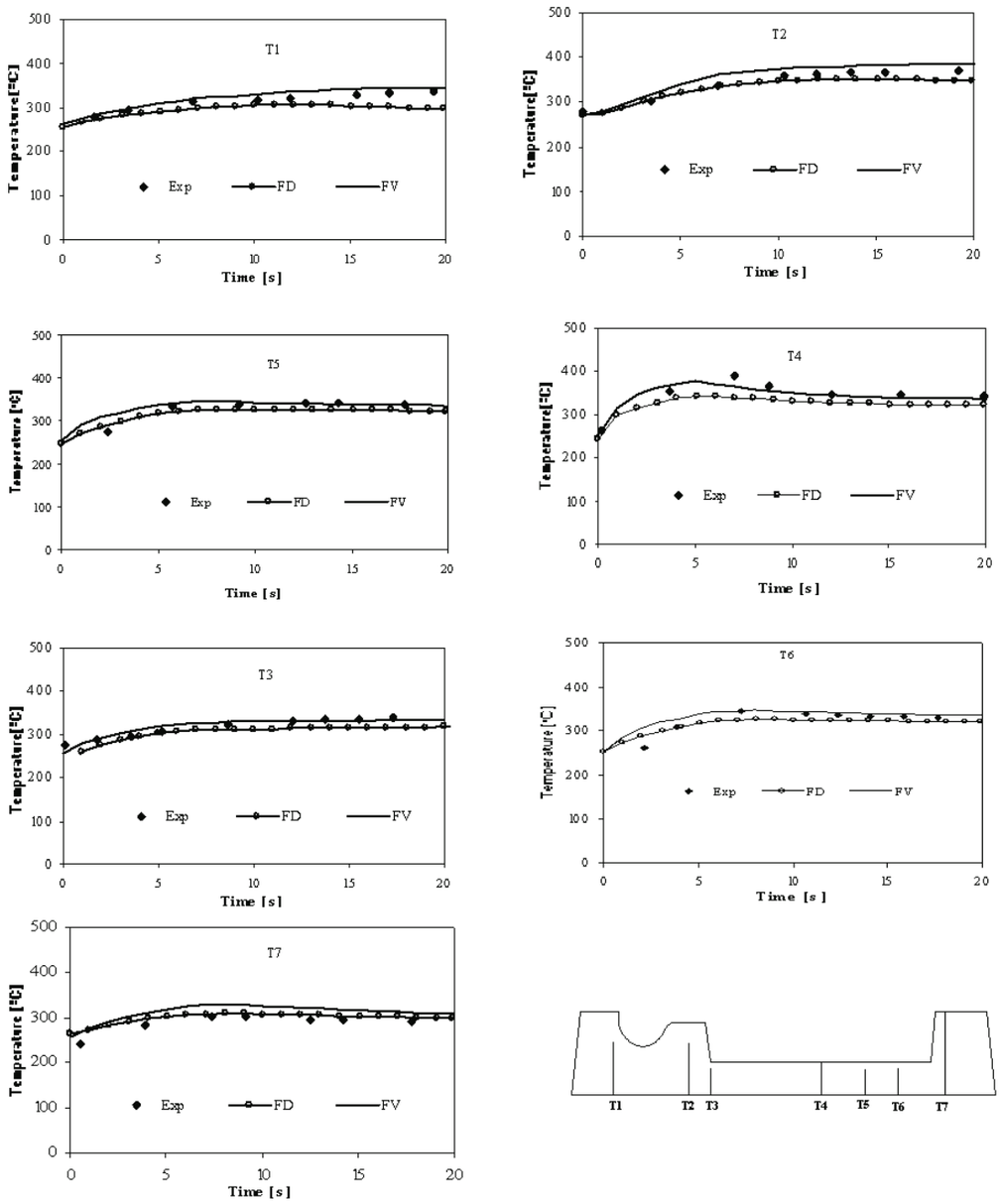

Fig. 10. Temperature results in seven points of the mold: Experimental measurement (Exp), Finite Differences numerical results (FD), Finite Volume numerical results (FV)

- straightforwardly programming.

In order to get even better results one could explore the grid refinement. However, special care must be taking in order to keep an acceptable computational time. This technique could also be an excellent choice for parallel computation, being each block or blocks affected to a physical processor.

While models can do a lot they are not yet transportable, meaning that considerable calibration is required for the conditions specific to the particular foundry. This is because nucleation

model are still highly empirical, and many physical properties are poorly known. Thus, we believe that the field has still potential for further development.

5. References

Beck, J.V. (1970). Nonlinear estimation applied to the nonlinear inverse heat conduction problem, *Int. J. Heat Mass Transfer*, 13, 703–716.

Beckermann, C. & Viskanta, R. (1988). Double-diffusion convection during dendritic solidification of a binary mixture, *Physicochem. Hydrodyn.*, 10, 195–213.

Bellet, M. & Fachinotti, V.D. (2004). ALE method for solidification modelling, *Comput. Methods. Appl. Mech. Engrg.*, 193, 4355–4381.

Bennon, W.D. & Incropera, F.P. (1987). A continuum model for momentum, heat and species transport in binary solid-liquid phase change systems-II. Application to solidification in a rectangular cavity, *Int. J. Heat Mass Transfer*, 30, 2171–2187.

Carslaw, H.S. & Jaeger, J.C. (1959). *Conduction of Heat in Solids*. Clarendon Press, Oxford.

Dimova, S.; Kaschiev, M.; Koleva, M. & Vasileva, D. (1998). Numerical analysis of radially nonsymmetric blow-up solutions of a nonlinear parabolic problem, *Journal of Computational and Applied Mathematics*, 97, 81–97.

Feldheim, V. & Lybaert, P. (2004). Solution of radial heat transfer problems with discrite transfer method applied to triangular meshes, *Journal of Computational and Applied Mathematics*, 168, 179–190.

Ferziger, J.H. & Peric, M. (1999). *Computational Methods for Fluid Dynamics*, 2nd edition, Springer Verlag, Berlin, Heidelberg, New York.

Ganesan, S. & Poirier, D.R. (1990). Conservation of mass and momentum for the flow of interdendritic liquid during 14. solidification, *Metall. Trans.*, 21B, 173–181.

Goodman, T.R. (1958). The heat balance integral and its applications to problems involving change of phase, *J. Heat Transf.*, 80(3), 335-341.

Knoll, D.A.; Vanderheyden, W.B.; Mousseau, V.A. & Kothe, D.B. (2001). On preconditioning Newton-Krylov methods in solidifying flow application, *SIAM, J. Appl. Math.*, 23(2), 381–397.

Lan, C.W. & Chen, F.C. (1996). A finite volume method for solute segregation in directional solidification and comparison with a finite element method, *Comput. Methods Appl. Mech. Engrg.*, 131(1–2), 191–207.

Lau, F.; Lee, W.B.; Xiong, S.M.; Liu, B.C. (1998). A study of the interface heat transfer between an iron casting and a metallic mould, *J. Mat. Process. Technol.*, 79 , 25–29.

Lightfoot, N.M.H. (1929). The solidification of molten steel, *Proc. Lond. Math. Soc.*, 31(2), 97-116.

Lockwood, F.C. & Shah, N.G. (1981). A new radiation solution method for incorporation in general combustion prediction procedures, *18th International Symposium on Combustion, The Combustion Institute, Pittsburgh, PA,* 1405–1414.

Monteiro, A.A.C. (1996). *Estudos do Comportamento Térmico de Moldações Metálicas para a Fundição Aplicando o Método das Diferenças Finitas Generalizadas*, Ph.D. Thesis, University of Minho, Braga, Portugal.

Monteiro, E. (2003). *Numerical study of the casting process using finite volume method*, M.Sc. Dissertation. University of Trás-dos-Montes e Alto Douro, Vila Real, Portugal.

Monteiro, E.; Monteiro, A.A.C. & Rouboa, A. (2006). Heat transfer simulation in the mould with generalize curvilinear formulation, *Journal of Pressure Vessel Technology*, 128, 462–466.

Monteiro, E. & Rouboa, A. (2005). Numerical simulation of the aluminium alloys solidification

in complex geometries, *J. Mech. Sci. Tech.*, 19(9), 1773–1780.
Ni, J. & Beckermann, C. (1991). A volume-averaged two-phase model for transport phenomena during solidification, *Metall. Trans.*, 22B, 349–361.
Norris, S.E. (2001). *A Parallel Navier Stokes Solver for Natural convection and Free Surface Flow*, Ph.D Thesis, Faculty of Mechanical Engineering, University of Sydney, Australia.
Pedroso, R.I. & Domoto, G.A. (1973). Inward spherical solidification-solution by the method of strained coordinates, *Int. J. Heat Mass Transf.*, 16, 1037-1043.
Peric, M. (1987). Efficient semi-implicit solving algorithm for nine-diagonal coefficient matrix, *Numer. Heat Transfer*, 11(3), 251–279.
Pina, H. (1995). *Métodos Numéricos*, McGraw-Hill.
Radovic, Z. & Lalovic, M. (2005). Numerical simulation of steel ingot solidification process, *J. Mater. Process. Technol.*, 160, 156–159.
Rappaz, M. (1989). Modelling of microstructure formation in solidification processes, *Int. Mater. Rev.*, 34, 93–123.
Rappaz, M. & Voller, V. (1990). Modeling of micro-macrosegregation in solidification process, *Metal. Trans.*, 21A, 749–753.
Rouboa, A.; Monteiro, E. & Almeida, R. (2009). Finite volume method analysis of heat transfer problem using adapted strongly implicit procedure, *J. Mech. Sci. Tech.*, 23, 1–10.
Santos, C.A.; Spim, J.A. & Garcia, J.A. (2003). Mathematical modelling and optimization strategies (genetic algorithm and knowledge base) applied to the continuous casting of steel, *Eng. Appl. Artif. Intelligence*, 16, 511–527.
Schneider, G.E. & Zedan, M. (1981). A modified Strongly Implicit procedure for the numerical solution of field problems, *Numer. Heat Transfer*, 4(1), 1–19.
Sciama, G. & Visconte, D. (1987). Modélisation des Transferts Thermiques Puor la Coulée en Coquillede Pièces de Robinetterie Sanitaire, *Foundarie, Fondeur d'Aujourd'hui,* 70, 11–26.
Sethian, J.A. (1996). *Level set methods and fast marching methods: evolving interfaces in computational geometry, fluid mechanics, computer vision and materials science*, Cambridge University Press.
Shamsundar, N. & Sparrow, E.M. (1975). Analysis of multidimentional condution phase change via the enthalpy model, *J. Heat Transfer*, 97, 333–340.
Shepel, S.E. & Paolucci, S. (2002). Numerical simulation of filling and solidification of permanent mold casting, *Applied Thermal Engineering*, 22, 229–248.
Shi, Z. & Guo, Z.X. (2004). Numerical heat transfer modelling for wire casting, *Mater. Sci. Eng.*, A265, 311–317.
Stone, H.L. (1968). Iterative solution of implicit approximations of multidimensional partial differential equations, *SIAM, J. Numer. Anal.*, 5, 530–558.
Swaminathan, C.R. & Voller, V.R. (1997). Towards a general numerical scheme for solidification systems, *Int. J. Heat MassTransfer*, 40, 2859 – 2868.
Tannehill, J.C.; Anderson, D.A. & Pletcher, R.H. (1997). *Computational Fluid Mechanics and Heat Transfer*, 2nd edition, Taylor & Francis Ltd.
Thompson, J.F.; Warsi, Z.U.A. & Mastin, C.W. (1985). *Numerical Grid Generation, Foundations and Applications*, Elsevier Science Publishing Co., Amsterdam.
Tryggvason, G.; Esmaeeli, A. & Al-Rawahi, N. (2005). Direct numerical simulations of flows with phase change, *Computers & Structures*, 83, 445–453.
Versteeg, H.K. & Malalasekera, W. (1995). *An Introduction to Computational Fluid Dynamics: The Finite Volume Method Approach*, Prentice Hall.

Viskanta, R. (1990). Mathematical modeling of transport processes during solidification of binary systems, *JSME Int. J.*, 33, 409–423.

Voller,V. R.; Brent, A. D. & Prakash, C. (1989). The modelling of heat, mass and solute transport in solidification systems, *Int. J. Heat Mass Transfer*, 32, 1719–1731.

Wang, G.X. & Matthys, E.F. (2002). Experimental ditermination of the interfacial heat transfer during cooling and solidification of molten metal droplets impacting on a metallic substrate: effect of roughness and superheat, *Int. J. Heat Mass Transfer*, 45, 4967–4981.

Wiwatanapataphee, B.; Wu, Y.H.; Archapitak, J.; Siew, P.F. & Unyong, B. (2004). A numerical study of the turbulent flow of molten steel in a domain with a phase-change boundary, *Journal of Computational and Applied Mathematics*, 166, 307–319.

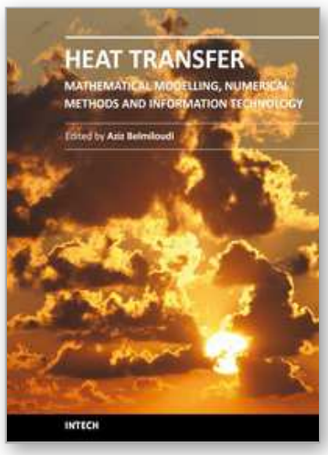

Heat Transfer - Mathematical Modelling, Numerical Methods and Information Technology

Edited by Prof. Aziz Belmiloudi

ISBN 978-953-307-550-1
Hard cover, 642 pages
Publisher InTech
Published online 14, February, 2011
Published in print edition February, 2011

Over the past few decades there has been a prolific increase in research and development in area of heat transfer, heat exchangers and their associated technologies. This book is a collection of current research in the above mentioned areas and describes modelling, numerical methods, simulation and information technology with modern ideas and methods to analyse and enhance heat transfer for single and multiphase systems. The topics considered include various basic concepts of heat transfer, the fundamental modes of heat transfer (namely conduction, convection and radiation), thermophysical properties, computational methodologies, control, stabilization and optimization problems, condensation, boiling and freezing, with many real-world problems and important modern applications. The book is divided in four sections : "Inverse, Stabilization and Optimization Problems", "Numerical Methods and Calculations", "Heat Transfer in Mini/Micro Systems", "Energy Transfer and Solid Materials", and each section discusses various issues, methods and applications in accordance with the subjects. The combination of fundamental approach with many important practical applications of current interest will make this book of interest to researchers, scientists, engineers and graduate students in many disciplines, who make use of mathematical modelling, inverse problems, implementation of recently developed numerical methods in this multidisciplinary field as well as to experimental and theoretical researchers in the field of heat and mass transfer.

INTECH
open science | open minds

InTech Europe
University Campus STeP Ri
Slavka Krautzeka 83/A
51000 Rijeka, Croatia
Phone: +385 (51) 770 447

InTech China
Unit 405, Office Block, Hotel Equatorial Shanghai
No.65, Yan An Road (West), Shanghai, 200040, China
中国上海市延安西路65号上海国际贵都大饭店办公楼405单元
Phone: +86-21-62489820

Fax: +385 (51) 686 166
www.intechopen.com

Fax: +86-21-62489821

IntechOpen